Published by IOP Publishing for Sissa Medialab

Received: *November 26, 2019*
Accepted: *December 23, 2019*
Published: *February 3, 2020*

Plasma Physics by Laser and Applications (PPLA 2019)
Physics Department, University of Pisa, Pisa, Italy
29–31 October, 2019

Acceleration of carbon ion beams by an ultraviolet laser under conditions relevant for ion fast ignition of inertial fusion

J. Badziak and J. Domański[1]

Institute of Plasma Physics and Laser Microfusion,
Hery Street 23, 01-497 Warsaw, Poland

E-mail: jaroslaw.domanski@ifpilm.pl

Abstract: The properties of carbon ion beams produced by a 100-kJ, 1-ps, KrF ultraviolet laser under conditions relevant for ion fast ignition (IFI) of DT fusion are numerically investigated using the 2D3V particle-in-cell code, and the possibility of achieving the ion beam parameters required for IFI is tested. The numerical simulations of carbon ion acceleration were carried out for flat carbon targets of various thicknesses (L_T) and for various laser beam apertures (d_L) on the target, while the laser pulse duration and energy were fixed. It was found that both the radiation pressure acceleration (RPA) mechanism and the sheath acceleration mechanism significantly affects the characteristics of the ion beam, with the RPA dominating in the case of thicker targets ($L_T \sim$ 10–30 μm). The ion beam parameters depend to a significant extent on the target thickness and the distance from the target. The mean and maximum ion energy decrease with the increase of L_T from 3 μm to 30 μm, while the ion beam intensity, the beam energy fluence and the total energy of the "useful part" of the ion beam (with an aperture ≤ 50 μm) reach maximum values at $L_T \sim$ 5–10 μm. For the optimal value of L_T and a small distance x from the target ($x \sim L_T$), the ion beam parameters are close to or higher than what is required for IFI. However, due to the angular divergence of the ion beam, the beam intensity and fluence decrease with an increase in the distance from the target, and at $x \geq 0.5$ mm the beam parameters are below the values required for fusion ignition. To reach these values, higher laser energies and/or more sophisticated schemes of ion acceleration are required.

Keywords: Accelerator modelling and simulations (multi-particle dynamics; single-particle dynamics); Ion sources (positive ions, negative ions, electron cyclotron resonance (ECR), electron beam (EBIS)); Accelerator Applications

[1]Corresponding author.

https://doi.org/10.1088/1748-0221/15/02/C02001

2020 JINST 15 C02001

Contents

2020 JINST 15 C02001

1 Introduction

Fast ignition (FI) [1–4] is an alternative approach to inertial confinement fusion (ICF) that differs from the conventional central-hot-spot ignition fusion [5, 6] by using separate drivers for the compression and ignition of the deuterium-tritium (DT) fuel. In this approach, a small part ($\sim 10^{-5}$ g) of DT fuel is compressed to about 1000 times the solid density ($\rho_f \sim 300\,\mathrm{g/cm^3}$) by a long-pulse (ns) driver (laser beams, X-rays), and then heated by an external ignitor to temperature ~ 10 keV. If the volume of the compressed fuel is sufficiently large (the confinement parameter $\rho_f r_f > 2\,\mathrm{g/cm^2}$), a thermonuclear burn wave ignited in the hot spot propagates through the fuel and so energy is produced. To compress the fuel, both direct-drive and indirect-drive approaches can be used. In the second approach, the X-rays can be produced by a laser, by a heavy ion beam from an accelerator, or by a Z-pinch [6]. As an ignitor, an intense short-pulse (picosecond) beam of fast electrons [1, 7–9], protons [2–4, 10–15], or ions [4, 16–22] can be used. Fast ignition has some potential advantages over conventional ICF, in particular: a higher energy gain, a lower overall driver energy, a reduction in compression symmetry requirements, and flexibility in using various compression drivers. However, the particle beam parameters required for ignition are extremely high, difficult to achieve using conventional accelerators, and the efficiency of energy transfer from the beam to the fuel should be high.

A promising option of FI is to use an ion/proton beam driven by a short-pulse multi-PW laser for the fuel ignition. Ion fast ignition (IFI) offers the well-controllable transport of ions from the ion source to the fuel, along with an efficient and localised deposit of ion energy to the fuel. The main challenge is achieving extremely high ion beam parameters and ion energy spectrum ensuring optimal ion energy range in the fuel, as well as reaching high ($> 10\%$) laser-to-ions energy conversion efficiency.

According to current knowledge, based mainly on numerical simulations performed at rather idealised assumptions for both the ion beam and the fusion (DT) target, the parameters of the ion beam required for the target ignition are as follows [3, 4, 19]: (a) beam intensity $I_b \sim 10^{20}\,\mathrm{W/cm^2}$, (b) fluence $F_b \sim 1\,\mathrm{GJ/cm^2}$, (c) beam energy $E_b \geq 10$ kJ, (d) duration of the ion pulse $\tau_b \sim 1$–10 ps,

(e) ion density $n_i \sim 10^{22}\,\mathrm{cm}^{-3}$, and (f) mean ion energy (in the beam with the narrowest possible spectrum) $E_i \sim 10$–$40\,\mathrm{MeV/amu}$.

To meet requirement (c) in the case of protons with a mean ion energy of ~ 5–$10\,\mathrm{MeV}$, the number of protons in the beam must be very large $\sim 10^{16}$. Since protons of such energies are usually produced by the target normal sheath acceleration (TNSA) mechanism [23–25] from a thin ($< 0.1\,\mu\mathrm{m}$) layer on the rear surface of the target, the size of the proton source enabling the production of 10^{16} protons must be large ($> 0.1\,\mathrm{mm}$), and the proton beam intensity and density at the source are much lower than the required. To meet requirements (a, b), the proton beam has to be highly focused to a spot several tens of micrometres wide, which is technically difficult. In addition, the focusing of the beam can be the source of an additional significant loss of beam energy (only part of the protons of the beam can be focused to the required spot). Another drawback is a broad (quasi-Maxwellian) energy spectrum of TNSA protons, which results in lengthening the ion pulse and decreasing its intensity during propagation from the source to the fusion target. In the case of using heavier ions for IFI such as carbon ions or vanadium ions [4], the number of accelerated ions can be considerably lower (by a factor of $\sim 10^2$ for C ions and $\sim 10^3$ for V ions) than for protons, because the required ion energies are considerably higher (several hundred MeV for C, and several GeV for V) [4]. Thus, both the volume and the transverse size of the ion source can be much smaller than the proton source. Furthermore, the acceleration of ions to sub-GeV (C ions) or GeV (V ions) energies requires laser intensities $\geq 10^{21}$–$10^{22}\,\mathrm{W/cm}^2$, considerably higher than those ensuring the generation of multi-MeV protons. At such laser intensities, the ion acceleration mechanisms other than TNSA can dominate the acceleration process. Among these, the mechanism referred to as radiation pressure acceleration (RPA) [24–28] or skin-layer ponderomotive acceleration (SLPA) [29]–[31] seems to be especially promising for producing ion beams relevant for IFI. In particular, for a target thick enough to ensure the required number of ions, the RPA mechanism can accelerate ions from the whole irradiated volume of the target and generate a high-energy, quasi-mono-energetic ion beam with a beam density and intensity up to several orders of magnitude higher than those for TNSA-driven proton beams [13, 25, 29, 31]. As a result, little to no focusing of the RPA-driven beam of C or V ions on the fusion target would be required. Thus, C or heavier ions accelerated by the RPA mechanism can be an attractive alternative to protons in IFI research.

In a real ion acceleration process, two or even more acceleration mechanisms can contribute to this process, and very often the RPA mechanism competes with the TNSA mechanism during the ion acceleration. For the production of ion beams relevant for IFI, the contribution of RPA to the acceleration process should be maximised, while TNSA should be minimised since it leads to the broadening of the ion energy spectrum and the reduction of the ion beam intensity. Because the radiation pressure increases proportionally to laser intensity, the contribution of RPA to the acceleration process grows with an increase in laser intensity. This contribution also depends on the irradiated target properties, as well as on the laser pulse contrast ratio (a high contrast ratio is preferred [32]) and the laser beam polarisation [24, 27, 28] and wavelength [33, 34]. The use of circular light polarisation [24, 27, 28] and/or a short-wavelength laser beam [33, 34] reduces the TNSA contribution to ion acceleration, while helping to reach the RPA-dominant regime of ion acceleration. In particular, using a high-intensity ($I_L \geq 10^{22}\,\mathrm{W/cm}^2$) circularly polarised (CP) ultraviolet (UV) laser beam as the ion beam driver seems to be an efficient way to produce ion beams with parameters required for IFI. In this case, a KrF excimer laser ($\lambda = 0.25\,\mu\mathrm{m}$) or a third harmonic

2020 JINST 15 C02001

of Nd:glass laser ($\lambda = 0.35\,\mu$m) could be a source of the UV laser beam accelerating the ions. The potential advantage of a KrF laser is its high energetic efficiency, as well as the ability to operate with the high repetition rates that are essential features of a laser driver in a fusion reactor. The use of a KrF laser to generate a dense plasma block for the fast ignition of DT fusion was considered in the paper [35], where the benefits of using such a laser instead of Nd:glass infrared laser for plasma block acceleration were demonstrated using hydrodynamic simulations. Unfortunately, the simulations were performed for very low laser pulse intensities ($\sim 10^{16}$ W/cm^2), several orders of magnitude lower than those required for IFI. To the best of our knowledge, there have been no studies on the UV-laser-driven acceleration of ions in laser-target interaction conditions relevant for IFI, and the properties of ion beams produced under such conditions are not well researched enough.

In this paper, the detailed properties of carbon ion beams driven by a 100-kJ, 1-ps, KrF ultraviolet laser are numerically investigated, and the possibility of attaining the ion beam parameters required for IFI is discussed. The numerical simulations were performed for realistic, relevant for IFI parameters of the laser pulse and a carbon target using a multi-dimensional (2D3V) particle-in-cell PICDOM code, which includes, in particular, the dynamic ionisation of the target and radiation losses due to synchrotron radiation produced by relativistic electrons. It was found that the ion beam parameters depend significantly on the target thickness L_T and the distance x from the target. At an optimal value of L_T and a small distance from the target ($x \sim L_T$), the ion beam parameters are close to or higher than what is required for IFI; however, at larger distances ($x \geq 0.5$ mm), desirable in real fusion systems, the beam parameters are below the values required for fusion ignition.

2 The numerical code and the laser and target parameters

The numerical simulations of carbon ion acceleration by a high-energy KrF laser were performed using a fully electromagnetic, relativistic multi-dimensional (2D3V) particle-in-cell PICDOM code [36], which includes, in particular, "on-line" calculations of the ionisation levels of the target atoms and accelerated ions [37–39], as well as radiation losses (RL) due to synchrotron radiation produced by relativistic electrons driven by the laser [40]–[44]. In the code, the process of ionisation is described using the Ammosov-Delone-Krainov formula [45–50], while the Sokolov model is used [51] to calculate the radiation losses (the radiation reaction force). However, due to very long computing time necessary for the planned simulations at the super-computer accessible by us (typically one month for a single set of the laser and target parameters), we had to simplify the code to perform the simulations in a reasonable time period and, as a result, the RL has not been included in the simulations.

In the simulations, a flat carbon target was irradiated by a circularly polarised 1 ps laser pulse with a wavelength equal to 0.25 μm, an energy of 100 kJ and a beam width (FWHM) $d_L = 15\,\mu$m or 10 μm (these parameters correspond to a laser pulse peak intensity equal to $4.63 \cdot 10^{22}$ W/cm^2 or $1.04 \cdot 10^{23}$ W/cm^2, respectively). The laser beam shape in time and space (along the y-axis) was described using a super-Gaussian function with a power index equal to 6. The target thickness (L_T) was equal to 3 μm, 6 μm, 12 μm, 18 μm or 30 μm, the target transverse size was equal to 18 μm or 25 μm and the carbon atom density in the target corresponded to diamond density (1.76×10^{23} atoms/cm^3). A pre-plasma with a density scale length of 0.3 μm and with a density shape described by an exponential function was placed in front of the target. The simulations were performed in the

2020 JINST 15 C02001

x, y space of dimensions $150 \times 31\,\mu m^2$. The space and time steps were equal to 20 nm and 4.44 as, respectively. The number of ion macro-particles was assumed to be 30 particles/cell.

3 Results and discussion

Based on numerical simulations carried out using the PICDOM code, we examined various characteristics of the generated ion beam and the dependence of these characteristics on the carbon target thickness for two laser beam widths (two beam intensities) at a given energy and duration of the laser pulse. The basic characteristics of the ion beam for fixed values of the target thickness ($L_T = 12\,\mu m$) and the laser beam width ($d_L = 15\,\mu m$) are shown in sub-section 3.1, while the dependence of these characteristics on the target thickness is discussed in sub-section 3.2.

3.1 Basic characteristics of the generated ion beam

The ionisation process of the target in the course of the laser pulse interaction with the target is illustrated in figure 1. The distribution of the ionisation level in the target is not homogenous and changes over time, right up to approximately 140 fs from the moment the laser starts interacting with the target. Once that time passes, the target is fully ionised, and the charge state of carbon atoms reaches the maximum possible value of $z = 6$. At the beginning of the interaction, the target is ionised by the electric field of the laser pulse, and then (after $t > 50$ fs) by the strong local electric field generated in the target by hot electrons partially separated from ions.

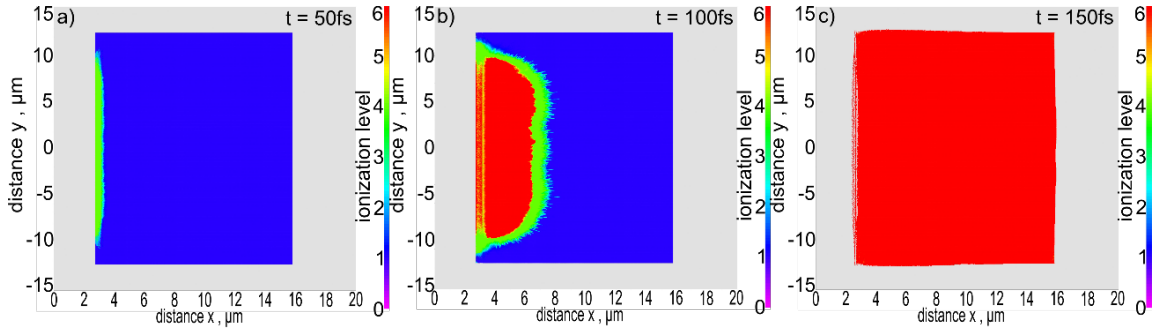

Figure 1. 2D spatial distributions of the ionisation level in the carbon target for different periods of the laser-target interaction. The target thickness $L_T = 12\,\mu m$, the laser beam aperture $d_L = 15\,\mu m$.

The spatial distributions of the ion density and the electric fields perpendicular to the laser beam axis E_y in the simulation region for the various stages of ion acceleration are presented in figure 2. In the initial stage of acceleration (prior to the maximum value of the laser pulse), a compact ion block with very high density (several times higher than the initial density of the target) is generated due to the laser light pressure. However, already at this stage of acceleration, heterogeneities in the ion block are clearly visible. Their main source is plasma instabilities arising in the area of direct interaction of the laser pulse with the target plasma. Possible mechanisms driving these instabilities are discussed, for example, in [52–54]. Throughout the further stages of acceleration, the ion beam structure becomes more and more complex and inhomogeneous, and its density decreases. In the final stage (at ~ 1.5 ps), the mean density of the high-energy ion beam in the simulation area drops to $n_i \sim 10^{22}\,cm^{-3}$. While the laser pulse interacts with the target ($t < 1.5$ ps), the ions are accelerated

2020 JINST 15 C02001

primarily by the RPA in the "hole boring" regime. After this interaction terminates, the ions are still accelerated by the electric field generated by hot electrons separated from the ions by laser-induced ponderomotive forces. Unfortunately, both at the RPA stage and the post-RPA stage, the ions are accelerated not only along the laser beam axis, but also in a radial direction and, as a result, the ion beam is angularly divergent (see figure 4).

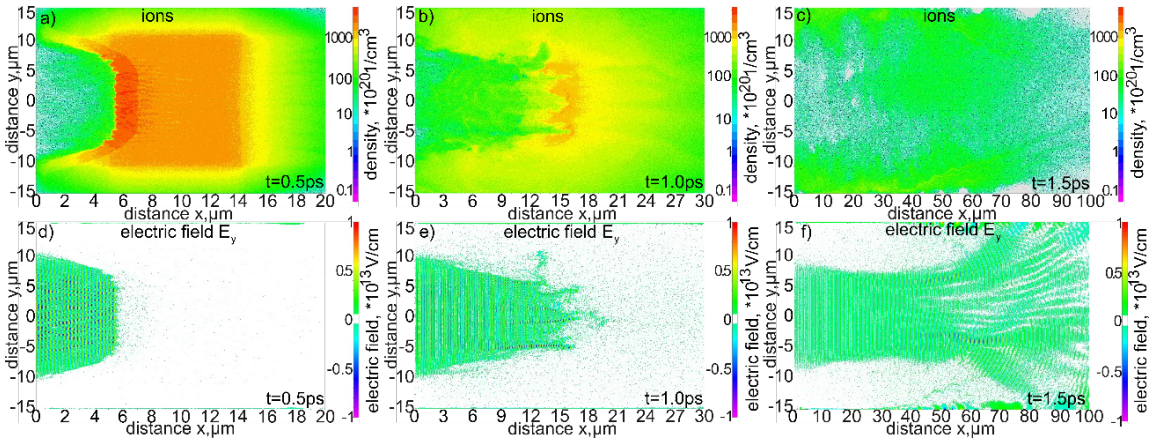

Figure 2. 2D spatial distributions of the ion density and the electric fields perpendicular to the laser beam axis E_y in the simulation region for various stages of ion acceleration. The target thickness $L_T = 12\,\mu m$, the laser beam aperture $d_L = 15\,\mu m$.

The energy spectrum of accelerated ions in the linear and logarithmic scale on the vertical axis is illustrated in figure 3. The spectrum is very wide, but has a distinct peak near 100 MeV. Mean ion energy of approximately 320 MeV is rather well suited to IFI requirements [4, 19], however the shape and width of the spectrum are far from optimal for IFI. In particular, a long high-energy tail present in the spectrum prevents the efficient and well-localized deposition of the ion beam energy into the fusion target. The main reason for this unfavorable shape of the energy spectrum is rather complex ion acceleration mechanism which, in addition to RPA, also includes TNSA and BOA [4] mechanisms. The latter seems to be responsible for the multi-GeV ions in the tail of the spectrum.

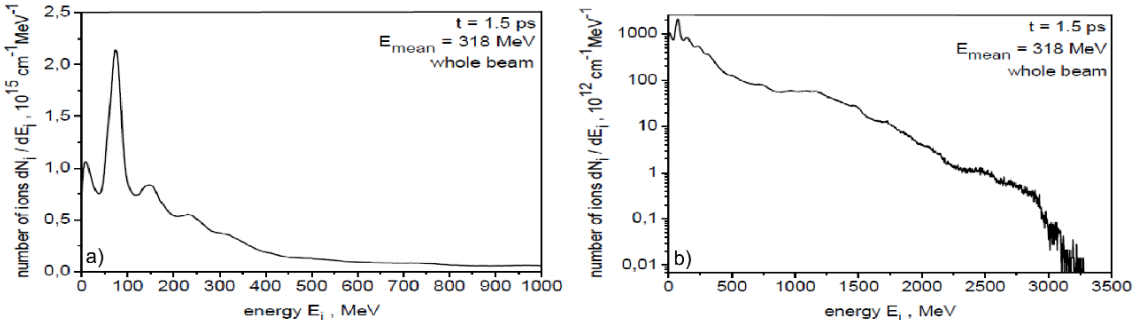

Figure 3. The energy spectra of C ions presented using the linear scale (left) and the logarithmic scale (right) on the vertical axis. $L_T = 12\,\mu m$, $d_L = 15\,\mu m$.

The angular and spatial distributions of ion beam intensity in the x-y plane recorded at a distance of 50 μm behind the target and at three different times: at the peak (read), the front slope (black)

2020 JINST 15 C02001

and the rear slope (blue) of the ion pulse are presented in figure 4. Both the angular distributions and the transverse distributions of beam intensity at various moments differ substantially. The ion beam with the smallest angular divergence and the narrowest transverse distribution is observed at the maximum of the ion pulse. However, even in this case, the effective angular divergence of the beam is quite significant (~ 20 deg), and the transverse size of the beam is around twice as large as the transverse size of the laser beam. It indicates the significant influence of radial ponderomotive forces on the ion acceleration process and formation of the ion beam.

The parameters specifying how to utilise the ion beam in IFI effectively are determined by its parameters in what is known as the far zone, i.e. at a distance from the ion target $x \gg d_L$. In the event that the ion beam is angularly divergent and/or the spectrum of ion velocities is wide (non-monochromatic), the characteristics of the ion beam in the far zone may differ significantly from the beam characteristics in the near zone ($x \sim d_L$). The temporal shape of the ion pulse recorded 50 μm, 100 μm and 500 μm behind the target is shown in figure 5 (the ion pulse intensity is averaged

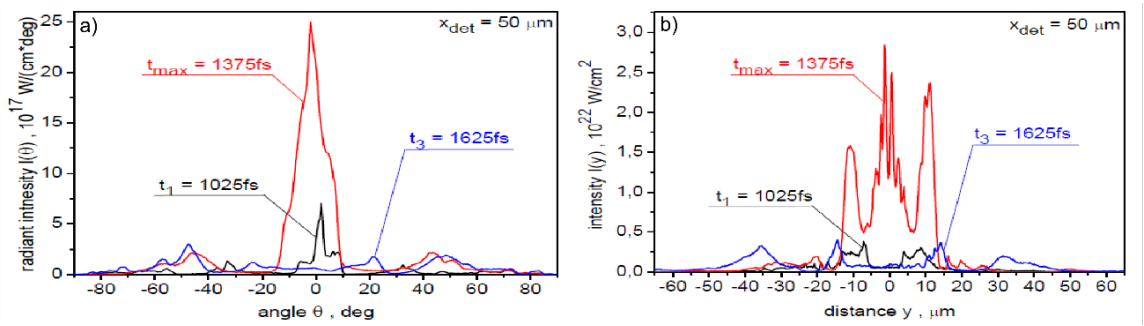

Figure 4. The angular (left) and spatial (right) distribution of ion beam intensity in the x-y plane recorded at a distance of 50 μm behind the target and for three different times: at the peak (red), the front slope (black) and the rear slope (blue) of the ion pulse. $L_T = 12$ μm, $d_L = 15$ μm.

over the area of aperture $d_c = 50$ μm). In turn, figure 6 presents the peak intensity and effective duration of the ion pulse, as well as the peak power and energy fluence (averaged over $d_c = 50$ μm) of the ion pulse as a function of the distance x from the target. While calculating the absolute values of the beam intensity, power and energy fluence in the far zone, the correction resulting from the three-dimensionality of the beam (3D correction) was taken into account, which is crucial in the case of angularly divergent beams. The 3D correction was also applied to determine other characteristics presented below. As can be observed, the ion pulses recorded at various distances from the target differ not only in peak intensity and duration, but also in shape. The duration of the ion pulse increases approximately linearly with the increase of the distance from the target, and the main reason for this is the dispersion of ion velocities. The peak intensity, the peak power and the energy fluence of the ion pulse decrease quite rapidly with the increase of x. The rapid drop in these values is the result of two factors: the angular divergence of the ion beam and the dispersion of ion velocities. It must be noted that the first factor plays a decisive role here. The values of the peak intensity required for IFI ($\sim 10^{20}$ W/cm^2) are attainable at distances smaller than ~ 0.5 mm from the target, while the required values of the peak power (> 10 PW) and energy fluence (~ 1 GJ/cm^2) are achievable only close to the target (at $x < 50$ μm).

2020 JINST 15 C02001

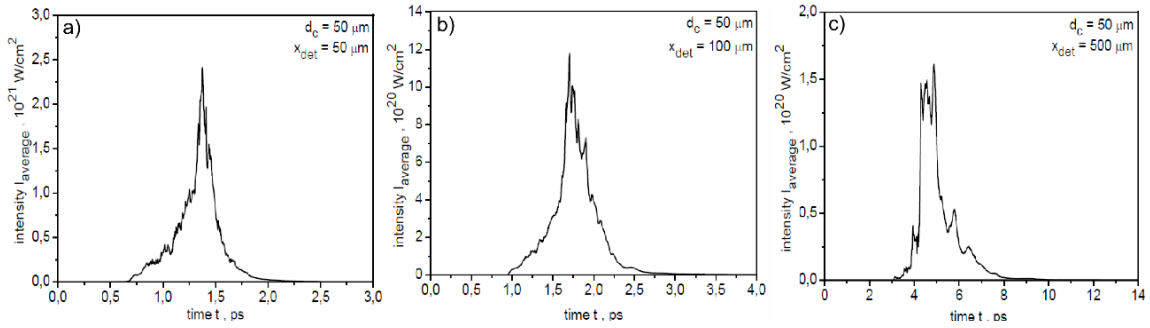

Figure 5. The temporal shape of the ion pulse recorded 50 μm (left), 100 μm (centre) and 500 μm (right) behind the target. In the calculations of absolute values of the ion pulse intensity at a long distance from the ion source, a correction related to the three-dimensional expansion of the ion beam was taken into account. L_T = 12 μm, d_L = 15 μm.

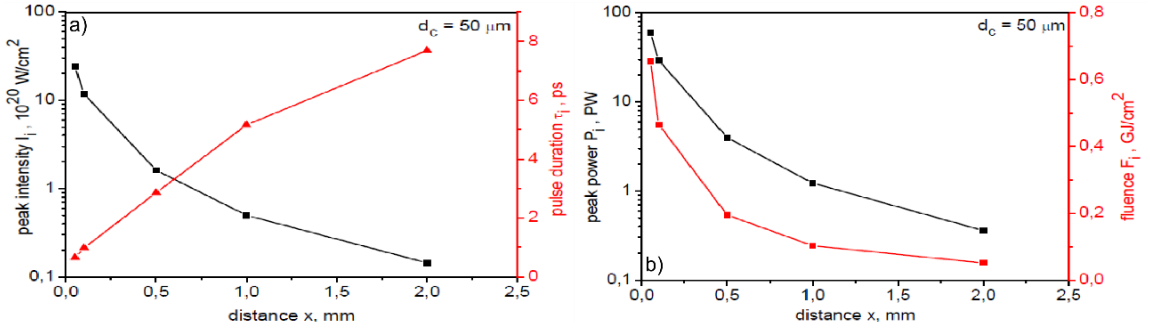

Figure 6. The peak intensity and duration of the ion pulse (left) as well as the peak power and energy fluence of the ion pulse (right) as a function of the distance x from the target. In the calculations of the above values, a correction related to the three-dimensional expansion of the ion beam was taken into account. L_T = 12 μm, d_L = 15 μm.

3.2 Dependence of characteristics of the ion beam on the target thickness

Figure 7 presents the dependence of mean and maximum ion energy, as well as the dependence of ion beam energy recorded in the aperture d_C = 50 μm on the target thickness for various distances x from the target. In that figure, the laser beam aperture for the thinner targets (of L_T = 3 μm, 6 μm and 12 μm) was assumed to be large, d_L = 15 μm, while for the thicker targets (of L_T = 18 μm and 30 μm) the beam aperture was smaller, d_L = 10 μm. Reducing the laser beam aperture to 10 μm, and, as a result, increasing the beam intensity for the thicker targets, was necessary to ensure the mean energy of accelerated ions possibly close to the values required for IFI, which for carbon ions are estimated to be ~ 300–600 MeV [4, 19]. It can be seen that the mean ion energy decreases with an increase in the target thickness at the fixed laser beam intensity, and that at 5 μm < L_T < 20 μm the mean energy is rather well matched to the values desirable for IFI. The observed decrease in the mean ion energy with the increase in L_T is primarily the result of the fact that thicker targets lead to laser energy being distributed to a larger number of accelerated ions. The total energy of central part of the ion beam, which could be considered as "useful" for the fusion target ignition (i.e. with an aperture ≤ 50 μm), relatively weakly depends on the target thickness, and for distances from the

2020 JINST 15 C02001

target < 0.5 mm reaches a maximum value at $L_T \sim 5$–10 μm. Here, the drop in the mean ion energy is partly compensated by the increase in the amount of accelerated ions. The total energy of the "useful" part of the ion beam reaches the values required for IFI (∼ 10 kJ) only at short distances from the target $x \leq 100$ μm.

The dependence of peak intensity and the duration of the ion pulse on the target thickness for various distances x from the target is shown in figure 8. As in the previous figure, the laser beam apertures for the thinner targets (3 μm, 6 μm and 12 μm) and the thicker targets (18 μm and 30 μm) are different and equal 15 μm and 10 μm, respectively. The peak intensity reaches a maximum value at $L_T \sim 5$–10 μm and even at distances $x \sim 0.5$ mm this value is higher than the value of the ion beam intensity required for IFI. The decreasing ion velocity is the reason for the increase in the ion pulse duration with increasing L_T seen in figure 8. The largest pulse extension is observed at large distances from the target, and at $x \sim 0.5$ mm the pulse duration varies from 1 ps to about 5 ps.

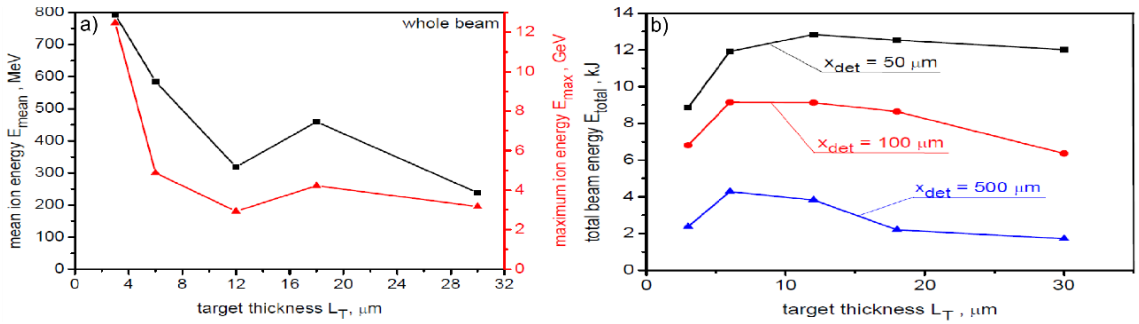

Figure 7. The dependence of the mean and maximum ion energy (left) as well as the dependence of the ion beam energy recorded in the aperture $d_C = 50$ μm (right) on the target thickness for various distances x from the target. For $L_T = 3$ μm, 6 μm and 12 μm, the laser beam aperture was $d_L = 15$ μm while for $L_T = 18$ μm and 30 μm, the laser beam aperture was $d_L = 10$ μm. In the calculations, a correction related to the three-dimensional expansion of the ion beam was taken into account.

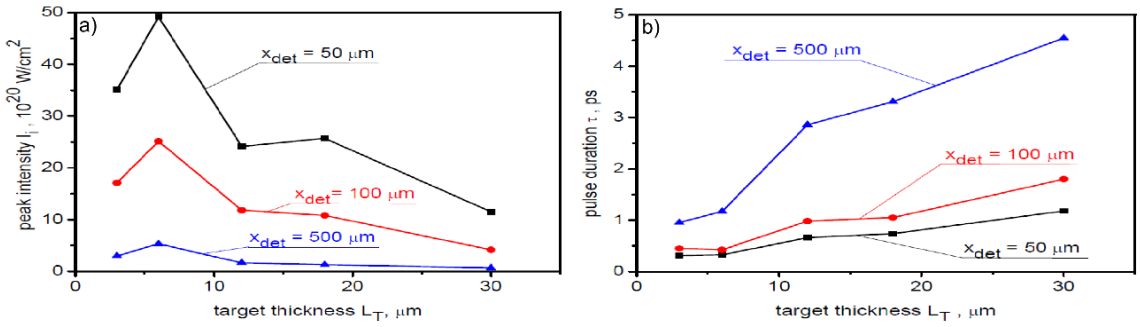

Figure 8. The dependence of peak intensity and the duration of the ion pulse on the target thickness for various distances x from the target. For $L_T = 3$ μm, 6 μm and 12 μm, the laser beam aperture was $d_L = 15$ μm, while for $L_T = 18$ μm and 30 μm, the laser beam aperture was $d_L = 10$ μm. In the calculations, a correction related to the three-dimensional expansion of the ion beam was taken into account.

As it was mentioned in the section 2, the radiation losses (RL) due to synchrotron radiation have not been included in our simulations. Based on the published results (e.g. [40, 42–44]), it could

2020 JINST 15 C02001

be expected that up to ~ 10–30% of the laser energy can be converted into RL at laser intensities assumed in the simulations. However, even at such high conversion efficiency of the laser energy to RL, a possible change in the ion beam parameters which are essential for IFI (mean ion energy, the beam intensity and fluence) should not be dramatic [41, 43, 44] and without affecting the main conclusions of our paper (below). Anyway, the ion beam parameters obtained in the simulations should be treated as the upper limit of these parameters for the laser-target conditions considered in the paper.

4 Conclusions

A KrF 100 kJ/1 ps laser efficiently accelerates carbon ions to the high energies required for IFI, but the parameters of the ion beam significantly depend on the target thickness (L_T) and the distance from the target (x). The mean and maximum ion energy decrease with an increase in the target thickness in the range from 3 μm to 30 μm, while the ion beam intensity, the beam energy fluence and the total energy of the "useful part" of the ion beam (with an aperture ≤ 50 μm) reach maximum values at L_T ~ 5–10 μm. For the optimal value of L_T and at a small distance from the target ($x \sim L_T$), the ion beam parameters are close to or higher than what is required for IFI. However, the ion beam intensity and fluence quickly decrease with an increase in the distance from the target due to the angular divergence of the beam, and at a distance x ≥ 0.5 mm the beam parameters are below the values required for fusion ignition. To reach the ion beam parameters required for IFI at realistic geometries of a fusion system, laser energies higher than 100 kJ and/or more sophisticated schemes of ion acceleration enabling a reduction in the angular divergence of the ion beam are necessary.

It is worth noting that although the ion beam parameters obtained under the considered conditions seem to be too low to initiate fusion ignition, these parameters are extremely high, not achievable in conventional accelerators. This creates the possibility of using these ion beams to explore new research areas in high energy density physics, nuclear physics and perhaps also in other fields.

Acknowledgments

This work was supported in part by the EUROfusion Consortium (the RoHGIFE project) and has received partial funding from the Euratom research and training programme 2014–2018 and 2019–2020 under grant agreement No. 633053. The simulations were carried out with the support of the Interdisciplinary Center for Mathematical and Computational Modelling (ICM), University of Warsaw under grant No. G57-20 and the Poznan Supercomputing and Networking Centre under grant No. 417.

References

[1] M. Tabak, J. Hammer, M.E. Glinsky, W.L. Kruer, S.C. Wilks, J. Woodworth et al., *Ignition and high gain with ultrapowerful lasers*, *Phys. Plasmas* **1** (1994) 1626.

[2] M.H. Key, *Status of and prospects for the fast ignition inertial fusion concept*, *Phys. Plasmas* **14** (2007) 055502.

[3] J. Badziak, S. Jabłoński and J. Wołowski, *Progress and prospect of fast ignition of ICF targets*, *Plasma Phys. Control. F.* **49** (2007) B651.

2020 JINST 15 C02001

[4] J. Fernández, B. Albright, F. Beg, M. Foord, B. Hegelich, J. Honrubia et al., *Fast ignition with laser-driven proton and ion beams*, *Nucl. Fusion* **54** (2014) 054006.

[5] J. Nuckolls, L. Wood, A. Thiessen and G. Zimmerman, *Laser compression of matter to super-high densities: Thermonuclear (CTR) applications*, *Nature* **239** (1972) 139.

[6] S. Atzeni and J. Meyer-ter-Vehn, *The Physics of Inertial Fusion*, Oxford University Press, Oxford (2004).

[7] P.A. Norreys, R. Allott, R.J. Clarke, J. Collier, D. Neely, S.J. Rose et al., *Experimental studies of the advanced fast ignitor scheme*, *Phys. Plasmas* **7** (2000) 3721.

[8] R. Kodama, H. Shiraga, K. Shigemori, Y. Toyama, S. Fujioka, H. Azechi et al., *Fast heating scalable to laser fusion ignition*, *Nature* **418** (2002) 933.

[9] J. Honrubia and J. Meyer-ter-Vehn, *Three-dimensional fast electron transport for ignition-scale inertial fusion capsules*, *Nucl. Fusion* **46** (2006) L25.

[10] M. Roth, T.E. Cowan, M.H. Key, S.P. Hatchett, C. Brown, W. Fountain et al., *Fast ignition by intense laser-accelerated proton beams*, *Phys. Rev. Lett.* **86** (2001) 436.

[11] M. Temporal, J.J. Honrubia and S. Atzeni, *Numerical study of fast ignition of ablatively imploded deuterium-tritium fusion capsules by ultra-intense proton beams*, *Phys. Plasmas* **9** (2002) 3098.

[12] M. Temporal, *Fast ignition of a compressed inertial confinement fusion hemispherical capsule by two proton beams*, *Phys. Plasmas* **13** (2006) 122704.

[13] J. Badziak, G. Mishra, N.K. Gupta and A.R. Holkundkar, *Generation of ultraintense proton beams by multi-ps circularly polarized laser pulses for fast ignition-related applications*, *Phys. Plasmas* **18** (2011) 053108.

[14] J. Honrubia, A. Morace and M. Murakami, *On intense proton beam generation and transport in hollow cones*, *Matter Radiat. Extremes* **2** (2017) 28.

[15] S. Weng, Z. Sheng, M. Murakami, M. Chen, M. Liu, H. Wang et al., *Optimization of hole-boring radiation pressure acceleration of ion beams for fusion ignition*, *Matter Radiat. Extremes* **3** (2018) 28.

[16] M.L. Shmatov, *Some problems related to heating the compressed thermonuclear fuel through the cone*, *Fusion Sci. Technol.* **43** (2003) 456.

[17] J.J. Honrubia and J. Meyer-ter-Vehn, *Fast ignition of fusion targets by laser-driven electrons*, *Plasma Phys. Control. F.* **51** (2008) 014008.

[18] C. Regan, T. Schlegel, V.T. Tikhonchuk, J.J. Honrubia, J.-L. Feugeas and P. Nicolaï, *Cone-guided fast ignition with ponderomotively accelerated carbon ions*, *Plasma Phys. Control. F.* **53** (2011) 045014.

[19] J. Davis, G.M. Petrov and T.A. Mehlhorn, *Generation of laser-driven light ions suitable for fast ignition of fusion targets*, *Plasma Phys. Control. F.* **53** (2011) 045013.

[20] J. Honrubia, J. Fernández, B. Hegelich, M. Murakami and C. Enriquez, *Fast ignition driven by quasi-monoenergetic ions: Optimal ion type and reduction of ignition energies with an ion beam array*, *Laser Part. Beams* **32** (2014) 419.

[21] S.M. Weng, M. Murakami, H. Azechi, J.W. Wang, N. Tasoko, M. Chen et al., *Quasi-monoenergetic ion generation by hole-boring radiation pressure acceleration in inhomogeneous plasmas using tailored laser pulses*, *Phys. Plasmas* **21** (2014) 012705.

[22] J.J. Honrubia and M. Murakami, *Ion beam requirements for fast ignition of inertial fusion targets*, *Phys. Plasmas* **22** (2015) 012703.

2020 JINST 15 C02001

[23] S.C. Wilks, A.B. Langdon, T.E. Cowan, M. Roth, M. Singh, S. Hatchett et al., *Energetic proton generation in ultra-intense laser–solid interactions*, *Phys. Plasmas* **8** (2001) 542.

[24] A. Macchi, M. Borghesi and M. Passoni, *Ion acceleration by superintense laser-plasma interaction*, *Rev. Mod. Phys.* **85** (2013) 751.

[25] J. Badziak, *Laser-driven ion acceleration: methods, challenges and prospects*, *J. Phys. Conf. Ser.* **959** (2018) 012001.

[26] T. Esirkepov, M. Borghesi, S. V. Bulanov, G. Mourou and T. Tajima, *Highly efficient relativistic-ion generation in the laser-piston regime*, *Phys. Rev. Lett.* **92** (2004) 175003.

[27] A. Macchi, F. Cattani, T.V. Liseykina and F. Cornolti, *Laser acceleration of ion bunches at the front surface of overdense plasmas*, *Phys. Rev. Lett.* **94** (2005) 165003.

[28] A.P.L. Robinson, M. Zepf, S. Kar, R.G. Evans and C. Bellei, *Radiation pressure acceleration of thin foils with circularly polarized laser pulses*, *New J. Phys.* **10** (2008) 013021.

[29] J. Badziak, S. Głowacz, S. Jabłoński, P. Parys, J. Wołowski and H. Hora, *Generation of picosecond high-density ion fluxes by skin-layer laser-plasma interaction*, *Laser Part. Beams* **23** (2005) 143.

[30] S. Głowacz, H. Hora, J. Badziak, S. Jabłoński, Y. Cang and F. Osman, *Analytical description of rippling effect and ion acceleration in plasma produced by a short laser pulse*, *Laser Part. Beams* **24** (2006) 15.

[31] J. Badziak, S. Jabłoński and S. Głowacz, *Generation of highly collimated high-current ion beams by skin-layer laser-plasma interaction at relativistic laser intensities*, *Appl. Phys. Lett.* **89** (2006) 061504.

[32] I.J. Kim, K.H. Pae, I.W. Choi, C.-L. Lee, H.T. Kim, H. Singhal et al., *Radiation pressure acceleration of protons to 93 MeV with circularly polarized petawatt laser pulses*, *Phys. Plasmas* **23** (2016) 070701.

[33] J. Badziak and S. Jablonski, *Ultraintense ion beams driven by a short-wavelength short-pulse laser*, *Phys. Plasmas* **17** (2010) 073106.

[34] J. Badziak and S. Jabłoński, *Acceleration of a solid-density plasma projectile to ultrahigh velocities by a short-pulse ultraviolet laser*, *Appl. Phys. Lett.* **99** (2011) 071502.

[35] R. Sadighi-Bonabi, H. Hora, Z. Riazi, E. Yazdani and S. Sadighi, *Generation of plasma blocks accelerated by nonlinear forces from ultraviolet KrF laser pulses for fast ignition*, *Laser Part. Beams* **28** (2010) 101.

[36] J. Domański and J. Badziak, *Generation of ion beams from a high-Z target irradiated by a laser pulse of ultra-relativistic intensity*, accepted for *Acta Phys. Polon.*

[37] G.M. Petrov, C. McGuffey, A.G.R. Thomas, K. Krushelnick and F.N. Beg, *Generation of heavy ion beams using femtosecond laser pulses in the target normal sheath acceleration and radiation pressure acceleration regimes*, *Phys. Plasmas* **23** (2016) 063108.

[38] J. Li, A.V. Arefiev, S.S. Bulanov, D. Kawahito, M. Bailly-Grandvaux, G.M. Petrov et al., *Ionization injection of highly-charged copper ions for laser driven acceleration from ultra-thin foils*, *Sci. Rep.* **9** (2019) 666.

[39] J. Badziak and J. Domański, *Towards ultra-intense ultra-short ion beams driven by a multi-PW laser*, *Laser Part. Beams* **37** (2019) 288.

[40] N. Naumova, T. Schlegel, V.T. Tikhonchuk, C. Labaune, I.V. Sokolov and G. Mourou, *Hole boring in a DT pellet and fast-ion ignition with ultraintense laser pulses*, *Phys. Rev. Lett.* **102** (2009) 025002.

[41] M. Tamburini, F. Pegoraro, A.D. Piazza, C.H. Keitel and A. Macchi, *Radiation reaction effects on radiation pressure acceleration*, *New J. Phys.* **12** (2010) 123005.

2020 JINST 15 C02001

[42] C.P. Ridgers, C.S. Brady, R. Duclous, J.G. Kirk, K. Bennett, T.D. Arber et al., *Dense electron-positron plasmas and ultraintense γ rays from laser-irradiated solids*, *Phys. Rev. Lett.* **108** (2012) 165006.

[43] R. Capdessus, E. d'Humières and V.T. Tikhonchuk, *Influence of ion mass on laser-energy absorption and synchrotron radiation at ultrahigh laser intensities*, *Phys. Rev. Lett.* **110** (2013) 215003.

[44] R. Capdessus and P. McKenna, *Influence of radiation reaction force on ultraintense laser-driven ion acceleration*, *Phys. Review* **E 91** (2015) 053105.

[45] A.M. Perelomov, V.S. Popov and M.V. Terent'ev, *Ionization of atoms in an alternating electric field*, *Sov. Phys. JETP* **23** (1966) 924.

[46] A.I. Nikishov and V.I. Ritus, *Ionization of atoms by an electromagnetic wave field*, *Sov. Phys. JETP* **25** (1967) 145.

[47] A.M. Perelomov, V.S. Popov and M.V. Terent'ev, *Ionization of atoms in an alternating electric field: II*, *Sov. Phys. JETP* **24** (1967) 207.

[48] A.M. Perelomov and V.S. Popov, *Ionization of atoms in an alternating electric field: III*, *Sov. Phys. JETP* **25** (1967) 482.

[49] M.V. Ammosov, N.B. Delone and V.P. Kraĭnov, *Tunnel ionization of complex atoms and of atomic ions in an alternating electromagnetic field*, *Sov. Phys. JETP* **64** (1986) 1191.

[50] M. Chen, E. Cormier-Michel, C. Geddes, D. Bruhwiler, L. Yu, E. Esarey et al., *Numerical modeling of laser tunneling ionization in explicit particle-in-cell codes*, *J. Comput. Phys.* **236** (2013) 220.

[51] I.V. Sokolov, J.A. Nees, V.P. Yanovsky, N.M. Naumova and G.A. Mourou, *Emission and its back-reaction accompanying electron motion in relativistically strong and QED-strong pulsed laser fields*, *Phys. Rev.* **E 81** (2010) 036412.

[52] V. Khudik, S.A. Yi, C. Siemon and G. Shvets, *The analytic model of a laser-accelerated plasma target and its stability*, *Phys. Plasmas* **21** (2014) 013110.

[53] A. Sgattoni, S. Sinigardi, L. Fedeli, F. Pegoraro and A. Macchi, *Laser-driven rayleigh-taylor instability: Plasmonic effects and three-dimensional structures*, *Phys. Rev.* **E 91** (2015) 013106.

[54] B. Eliasson, *Instability of a thin conducting foil accelerated by a finite wavelength intense laser*, *New J. Phys.* **17** (2015) 033026.

2020 JINST 15 C02001